coatings

Article

Verification of the Non-Axisymmetric Deformation Mechanism of Bearing Rings after Quenched in a Multi-Field Coupled Simulation

Qian Liu [1], Dongying Ju [2,*], Xusheng Li [2], Kousuke Ishikawa [3], Rui Lv [3], Weifeng Lian [4] and Min Zhang [4]

1 School of Materials and Metallurgy, University of Science and Technology Liaoning, Anshan 114051, China; tclan1987@163.com
2 Saitama Institute of Technology, Fukaya 369-0293, Japan; i1004hxu@sit.ac.jp
3 Tokyo Green Power Electric Technology, Co., Ltd., Tokyo 111-0022, Japan; ishikawa@gpower.jp (K.I.); rui@gpower.jp (R.L.)
4 Changzhou NRB Corporation, Changzhou 213022, China; weifeng.lian@nrb.com.cn (W.L.); zm@nrb.com.cn (M.Z.)
* Correspondence: dyju.sitec@gmail.com

Abstract: In this paper, the elliptical deformation mechanism of the bearing ring after quenching has been studied by using the theory of "metal-thermal-mechanical" and the multi-field coupling simulation method. It has been mainly considered that it occurred as an experimental phenomenon in the past that, when the bearing ring had been oil quenched, a vapor film had usually formed on its surface, and the breakage and boiling of the vapor film had been observed to be uneven in a circumferential direction. For this reason, based on the phase transition kinetics, several types of heat transfer boundary conditions on the outer surface of bearing rings during oil quenching have been assumed, and the multi-field coupled simulation of the quenching process of bearing rings has been carried out in this paper. According to the simulation results, it could be concluded that when two different heat transfer boundary conditions have been set on the outer surface of the bearing outer ring in the form of orthogonal symmetry, the quenched bearing outer ring would produce elliptical deformation. The above simulation results have been basically verified by comparing the experimental results.

Keywords: oil quenching; heat transfer; mechanism of elliptical deformation; multi-field coupled simulation

check for updates

Citation: Liu, Q.; Ju, D.; Li, X.; Ishikawa, K.; Lv, R.; Lian, W.; Zhang, M. Verification of the Non-Axisymmetric Deformation Mechanism of Bearing Rings after Quenched in a Multi-Field Coupled Simulation. *Coatings* **2022**, *12*, 676. https://doi.org/10.3390/coatings12050676

Academic Editors: Petrică Vizureanu and Emerson Coy

Received: 28 February 2022
Accepted: 9 May 2022
Published: 15 May 2022

1. Introduction

Bearings have already been an indispensable core component in many areas, such as aerospace, high-speed rail, and automotive. In practical application, bearings have been designed to withstand cyclical loads and resist external shocks. The purpose has provided an important guarantee for the high rotational accuracy and high wear resistance of many rotary machines at high speeds. Therefore, the service life and rotation accuracy of all rotating machinery has closely related to these characteristics of bearings. In the manufactured process of bearings, metallurgy, and the preparation of the material, the processing technology of materials, and heat-treatment technology have been the main factors that affected bearing performance [1]. Among them, the quenching process of the bearing ring has been very important to determine the final strength, wear resistance, rotation accuracy, and rotation noise performance of bearing rings, because the heat-treatment process of the bearing ring resembles close to the last process of bearing parts production [2,3].

The heat-treatment process of the bearing ring has been mostly carried out by oil quenching. The heat transfer process on each surface of the parts has been very complicated. After being heated, nucleate boiling occurred in the cooling medium, the vapor film adheres to the surface of the part, and finally, decomposed and boiled [4]. At the same time, several types of heat transfer have appeared, including latent heat of phase transition. These phenomena caused inelastic thermal deformation during oil quenching.

On the other hand, after the oil is quenched, the bearing ring often produces elliptical deformation, which can cause adverse effects on the rotation accuracy of the bearing. Even if the elliptical deformation has been eliminated by subsequent machining, the surface hardness can be uneven, and the strength and wear resistance of the surface can be decreased. Therefore, the value of ellipticity is one of the important detection indices of the bearing ring after the oil is quenched. However, how does elliptical deformation occur? This question has not been answered, nor verified accurately and reliably.

Simulation has usually been used in the process of heat-treatment analysis to explain the complex phenomena and interactions of multi-field coupling. Professor Inoue and Ju put forward the phase transition mechanics theory and developed heat-treatment simulation software (COSMAP) with a multi-field coupled function, according to the theory [5]. In recent years, COSMAP has been applied to solve many types of heat-treatment engineering problems [6–11]. Xusheng Li et al. simulated a steel gear model based on the measured phase-change plasticity parameters and the metal-thermal-mechanical theory. Transformation plasticity reflects an important distortion behavior of alloy steel materials during the carburizing and quenching heat-treatment process. To reveal the densification behavior and material properties of transformation plasticity, the method proposed for the precise measurement of distortion behavior under rapid cooling is a very effective and practical experimental technique [12]. Jiangang Wang et al. studied the carburizing and quenching process of helical gear by combining an experiment with a numerical simulation. Based on the theory of metal thermodynamics, they proposed the vapor film located at the outer end surface ruptured preferentially, and the temperature changed dramatically—the position of the inner end face is close to the center, the vapor film is finally broken, and the temperature changes slowly. This temperature difference results in different simultaneity of the microstructure transition, resulting in uneven thermal stress and microstructure stress of the gear. The effect of this stress on the gear is characterized by uneven deformation after quenching [13]. Li Minglei proposed to reduce the equivalent stress and make the radial deformation more uniform by changing the structure of the outer surface of the outer ring of the bearing research [14]. Y. Shao, W. Peng, and S. Chen carried out that the cold treatment process can accelerate the transformation from retained austenite to martensite in the bearing ring, reduce the content of retained austenite, refine the martensite structure and promote the precipitation of network carbide, significantly improving the residual stress on the bearing ring surface while reducing the deformation with the cold treatment process added to the heat treatment [15]. Zhaoxi Cao, etc., explored high carbon bearing steel of GCr15 (100Cr6); double quenching refined both carbides and prior austenite grain sizes and enhanced the RBF-strength and RCF-life [16]. Xiaohui Lu, etc., optimized the quenching process and added a prior pre-quenching process; the enhanced toughness was attributed to the nanometric martensite-bainite duplex microstructures and the formation of film-like retained austenite [17]. Kai Zhu, etc., indicate that the medium temperature affects residual stress inside the thick plate significantly during the immersion quenching process; the pre-stretching treatment can effectively reduce residual stresses within the thick plate [18]. H.Y. Wu, etc., studied a novel spheroidizing annealing treatment, with the increase of the spheroidization degree and the decrease in the cementite particle size in the initial microstructure; the particle size of undissolved carbide decreases, compared with the traditional off-line isothermal spheroidizing annealing, and thus, the properties of the wear and contact fatigue of the samples were improved [19].

However, up to now, the elliptical deformation of the bearing ring after quenching has rarely been studied and analyzed, especially since the elliptical deformation principle of the bearing ring after quenching has not been reasonably explained. Therefore, in order to explore the elliptical deformation principle of bearing ring quenching, this paper adopted the theory of “metal-heat-mechanics” and the multi-field coupled simulation method to verify the elliptical deformation principle during bearing ring quenching. In particular, it has been found by access to information that the vapor film formed on the outer surface is uneven during bearing ring oil quenching, and the vapor film, which ruptures and boils, is unevenly distributed in the circumferential direction [4]. The result has aroused concern, and it has been considered that it may be the main cause of the elliptical deformation of the bearing ring. For this reason, several types of heat transfer boundary conditions on the outer surface of bearing rings during oil quenching have been assumed, especially, it has been assumed that when two different heat transfer boundary conditions have been set on the outer surface of the bearing outer ring, in the form of orthogonal symmetry, the purpose is to simulate a non-uniform distribution of the vapor film rupturing and boiling. This is carried out with a multi-field coupled simulation of the bearing ring oil-quenching process. Through the comparison of simulation results and the measurement results of the bearing outer ring ellipse deformation in the experiment, it is verified that the above judgment is the factor leading to the bearing outer ring elliptical deformation. It is often very difficult to determine, however, the heat transfer behavior and heat transfer coefficient of the outer surface of the bearing in this complex set of circumstances. The article proposed the use of inverse analytical and visual analysis methods to obtain the heat transfer coefficients on the surface of steel parts during quenching. Based on the process of oil-film formation and rupture captured by a high-speed camera, three heat transfer models are assumed. Combined with the experimental results, the mechanism of the non-axisymmetric deformation of the bearing outer ring is verified.

2. Experimental Procedure

2.1. Heat-Treatment Process

Figure 1a is a partial drawing of the bearing outer ring analyzed. The specimen material was bearing steel GCr15 (B00150) and GB/T 18254-2002. Figure 1b shows the bearing outer ring heat-treatment process flowchart, including heating, holding, and quenching. This analysis has not included the tempering process. The quenching equipment is an RC-160 mesh belt furnace—a furnace with dimensions of 6700 mm × 800 mm × 90 mm and a quenching bath dimension of 16 cubic meters. The quenching oil was the applied LP Hi-Temp 80M bright quenching oil. The first step of the heat treatment was placed into the mesh belt furnace to heat. The temperature of each zone was set at 845 °C, the heating time was 15 min. A total of 60 L/min nitrogen and 20 mL/min methanol gas were passed through heat, with the purpose, respectively, of driving out the air in the furnace and reducing the occurrence of decarbonization. The second step was carried out with the furnace insulation so that the specimen was uniformly austenized. Finally, the quenching process was performed, and the oil temperature was set to 60 °C.

After the bearing outer ring was quenched, the ellipticity value of the specimen was tested by using a D913A bearing gauge, it was mainly measured at the quarter height, half-height, and three-quarters height of the quenched specimen, the experimental results are shown in Table 1.

Table 1. Bearing outer ring elliptical deformation measurement results in the experiment (mm).

Z Variation	First Experiment	Second Experiment	Third Experiment	Experimental Average Value
3/4H	0.11	0.10	0.08	0.096
1/2H	0.11	0.10	0.07	0.093
1/4H	0.10	0.07	0.08	0.083

It is shown that the quenched specimen presented an elliptical shape and that the ellipticity values were closer in the height direction, reflecting their more uniform deformation in the height direction than the circumferential direction. Therefore, the selection of the process and the cooling medium were more appropriate.

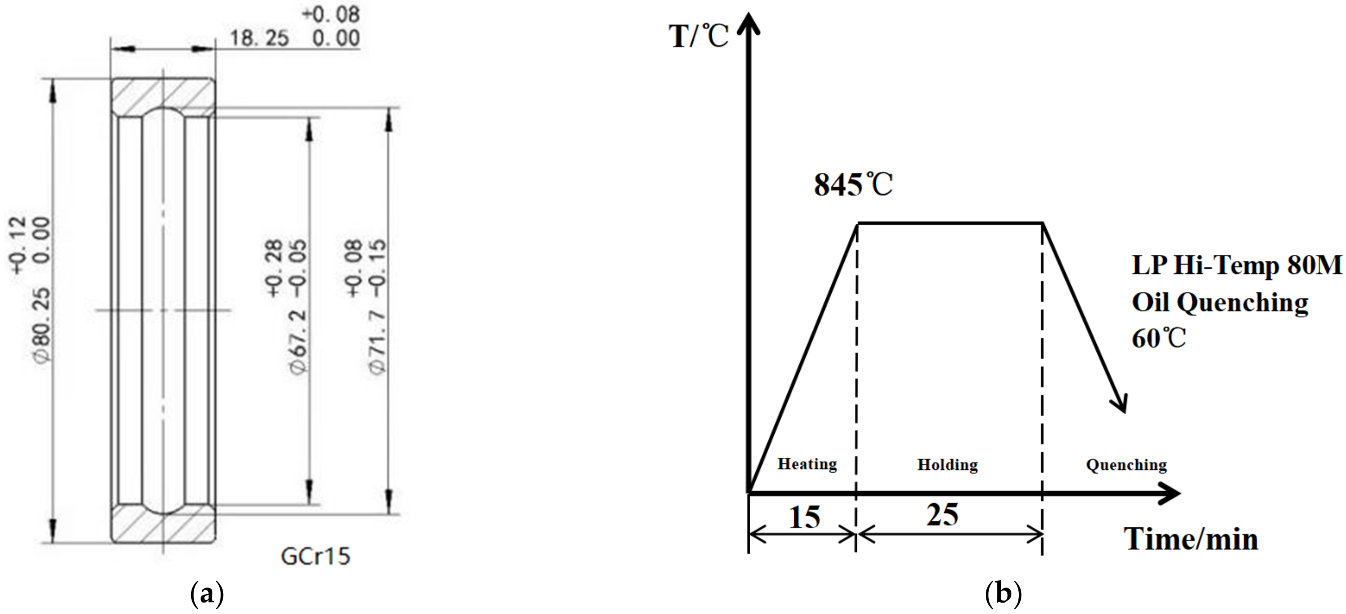

Figure 1. Part drawing of bearing outer ring and heat-treatment condition. (**a**) Part drawing of bearing outer ring; (**b**) heat-treatment process of GCr15.

The hardness of the bearing outer ring before and after quenching was measured by the Shanghai HengYi HM500 hardness tester. The hardness results are shown in Table 2. It can be seen from the results that the hardness of the outer surface, internal surface, and inner surface of the bearing outer ring is significantly improved; the hardness values of the outer surface, internal surface, and inner surface are basically the same, and the parts are hardened.

Table 2. Bearing outer ring outer surface hardness results in the experiment (HV).

Number	Outer Surface before Quenching	Outer Surface after Quenching	Internal Surface before Quenching	Internal Surface after Quenching	Inner Surface before Quenching	Inner Surface after Quenching
1	189	792	192	795	195	802
2	192	795	190	795	195	793
3	190	793	190	794	193	802
Average	190.33	793.33	190.67	794.67	194.33	800.67

For the test sample inlay using acrylic resin cold inlay, the sample was mechanically ground, polished with a selected 2.5 µm diamond suspension, and polished for 3 min after 4% nitric acid alcohol corrosion. The organization of each surface before and after quenching is shown in Figure 2.

The microstructure of the outer surface layer, inner surface layer, and neutral layer before quenching present punctate, fine-grained, spherical pearlite tissue. The microstructure of the outer surface layer, inner surface layer, and neutral layer after quenching present fine-grained martensite, crypto-grained martensite, retained carbides, and retained austenite. The parts show a relatively high-quality quenched structure.

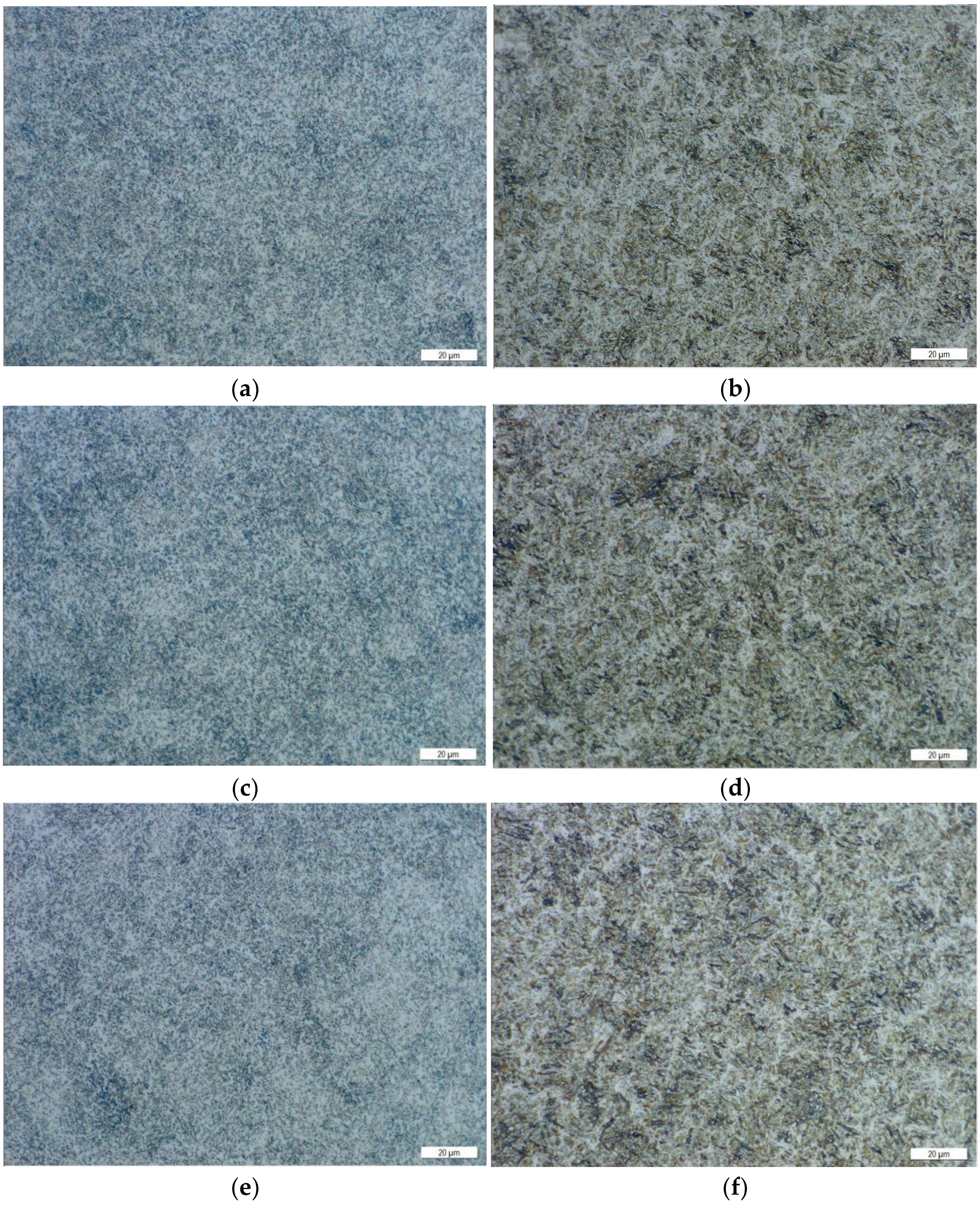

Figure 2. Microstructure of the surface layer before and after quenching. (**a**) Organization of inner surface layer before quenching; (**b**) organization of inner surface layer after quenching; (**c**) organization of neutral layer before quenching; (**d**) organization of neutral layer after quenching; (**e**) organization of outer surface layer before quenching; (**f**) organization of outer surface layer after quenching.

2.2. Measurement of Cooling Curves

The heat transfer process around the bearing outer ring is very complex when the bearing outer ring is quenched using quench oil. It is often accompanied by nucleation boiling of the hot fluid, generation of a vapor film on the outer surface of the bearing outer ring, and film boiling and convection phenomena of the hot fluid as the vapor film is peeled off. In particular, it is often very difficult to determine the heat transfer behavior and heat transfer coefficient of the outer surface of the bearing in this complex set of circumstances. However, if the heat transfer coefficient of the outer surface of the bearing cannot be correctly assimilated, it is also impossible to simulate the temperature field, stress–strain field, and changes in the internal metal structure of the bearing. Therefore, in this thesis, in order to assimilate the heat transfer coefficient of the outer surface of the bearing during quenching, a method is proposed in which two 1.1 mm holes are machined orthogonally (90°) in the outer ring of the bearing, as shown in Figure 3, and then a 1 mm diameter K-type thermocouple is inserted into the top of the holes. Since the thermocouple is soldered with silver paste inside the holes, which are only 0.01 mm from the outer surface, the measured cooling curve, with a high degree of accuracy, can be achieved. The measurement device is shown in Figure 4. The measured cooling curve is shown in Figure 5. Moreover, ch1 and ch2 in Figure 4 represent the temperature change curve detected by thermocouples in different directions. If the height direction is defined as the Z direction, ch1 is the detection point in the X direction of the ring, and ch2 is the detection point in the Y direction of the ring. Our current aim is to first solve the practical problem of obtaining the cause of the oval shape of the bearing outer ring after quenching. From this point of view, our proposed heat transfer coefficient scheme was substituted into the multi-field coupled simulations to obtain elliptical deformation results that are reasonable and close to the experimental results. We are aware of the uncertainties associated with this approach. In order to guarantee the experimental accuracy, we performed four cooling curve tests under the same process conditions, and the experimental results show a highly reappeared cooling rate curve. The cooling rate curves have been calculated according to the cooling curves, as shown in Figure 6. The cooling rate was calculated with the initial data in order to show the validity of the experimental tests because the cooling experiments showed a highly reappeared cooling rate curve. We can see from the measured cooling curve that the cooling curve and the cooling rate (gradient) are completely different in the two orthogonal directions. This indicates that the outer ring of the bearing produces a completely different heat transfer near the outer surface of the bearing due to the complex phenomenon of the thermal fluid (quenching oil) during the quenching process. This results in a large difference in the cooling in the two orthogonal directions. This is, of course, a very interesting phenomenon, and further visualization studies are needed to explain the mechanism of the problem.

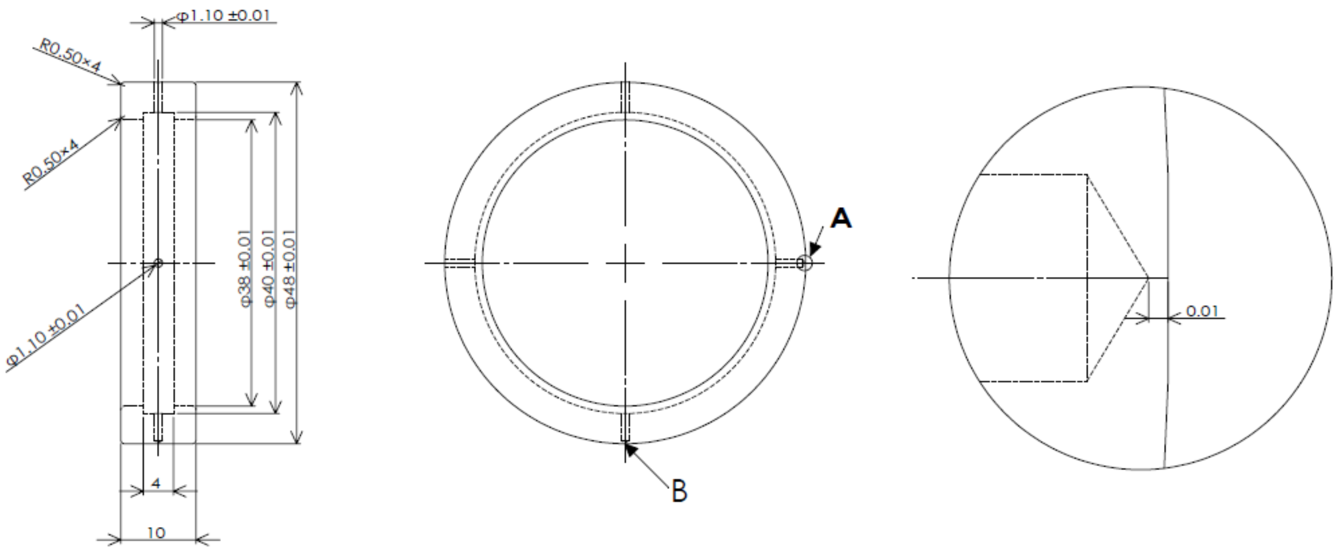

Figure 3. Measurement of specimens for cooling curves at the outer edge of the bearing. A and B are the location of the K-type thermocouple device.

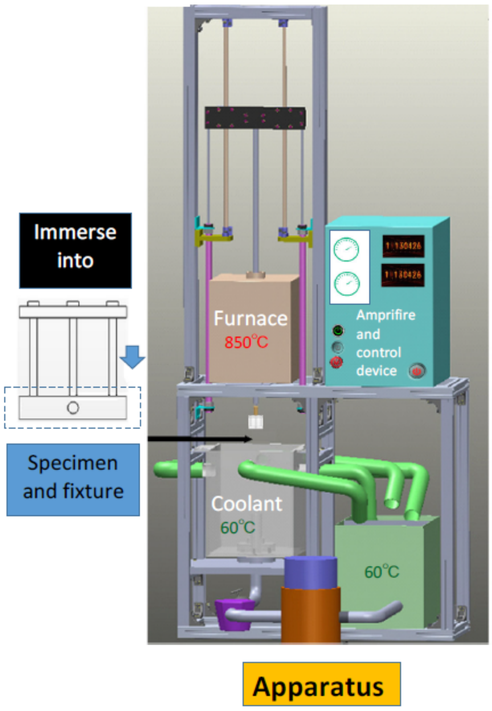

Figure 4. Measurement equipment.

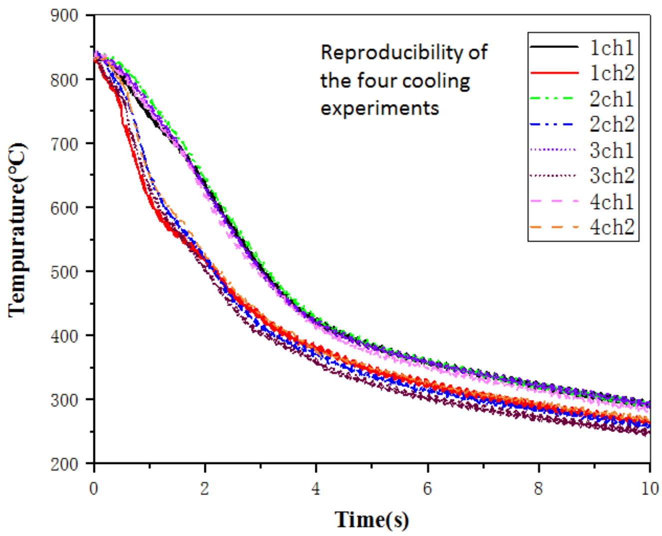

Figure 5. Measurement results of the cooling curves.

2.3. Identification of Heat Transfer Coefficient

When a flowing fluid comes into contact with the surface of a flat plate, the rate of heat transfer from the solid body to the fluid is proportional to the surface area of the solid in contact with the fluid, and the temperature difference between them. The convective heat transfer coefficient can be expressed by an equation called Newton's law of cooling. The heat transfer coefficient is a mathematical explanation of the temperature difference between the fluid and the surface of the solid that arises from the movement of the fluid:

$$\mathrm{Q} = \mathrm{hA}(T_s - T_\infty) \quad (1)$$

where Q is the rate of heat transfer; h is the convective heat coefficient; A is the surface area of the solid; T_s is the temperature of the solid surface; T_∞ is the temperature of the fluid. On the other hand, if the thermal resistance due to heat conduction (internal resistance) is sufficiently smaller than the resistance due to heat transfer coefficient at the surface (external resistance), then the temperature distribution inside the specimen can be considered to be almost uniform. In this case, the amount of heat from the specimen surface is obviously equal to the decrease in internal energy, which means that the following Equation (2) holds.

$$Q = \mathrm{hA}(T_s - T_\infty) \doteq -\rho CV\frac{dT_s}{dt} \tag{2}$$

where V is the volume of the test specimen, C is specific heat, ρ is density. Therefore, although it is difficult to measure the heat transfer coefficient h of the rapidly cooling bearing surface, the heat transfer coefficient can be obtained by substituting the measured cooling curve and cooling rate into the above equation. In other words, this method is the concentrated heat capacity method [4,20].

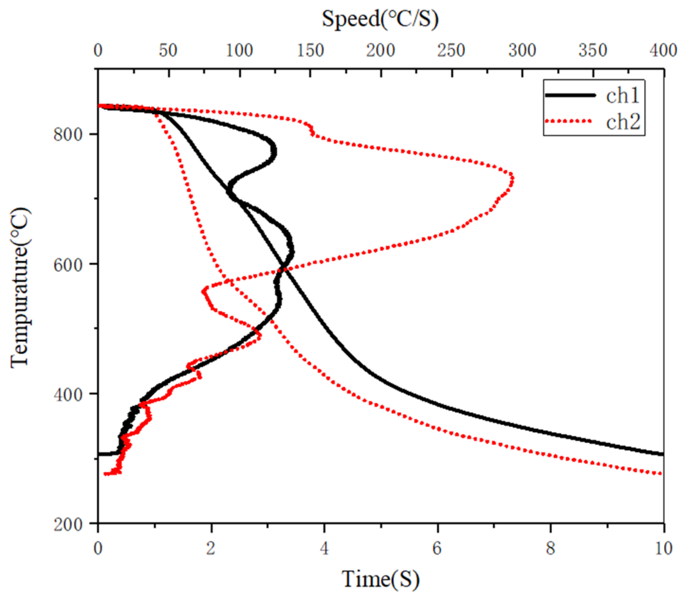

Figure 6. Calculated results of the cooling rate curves.

2.4. Numerical Simulation Program

In order to explore the elliptical deformation principle of bearing ring quenching, the theory of "metal-heat-mechanics" has been adopted along with the multi-field coupled simulation method to verify the elliptical deformation principle during bearing ring quenching. A finite element program called COSMAP had been developed to predict the temperature field and analyze the elliptical deformation of the quenched bearing ring principle [5]. COSMAP is a finite element program that simulated the diffused field of carburizing and nitriding during heat treatment, the temperature field based on heat conduction and phase transformation, and the interaction of inelastic stress/strain fields during heat treatment. The theory of the program and the governing equation of multi-field coupling can be found in reference [5]. Due to space limitations, this article has only given an introduction to the heat transfer equation.

Based on the first law of thermodynamics, the conservation of energy, the increment of internal energy is equal to the sum of the heat energy transferred, the work done and the latent heat of phase transformation. The physical equation can be formulated [7–10] as:

$$\rho c\dot{T} = \frac{\partial q_I}{\partial \chi_I} + \sigma_{ij}\varepsilon_{ij}^p - \sum \rho_I l_I \dot{\xi}_I \tag{3}$$

where, ρ, c denotes the density and the specific heat. $\sigma_{i\,j}$, ε_{ij}^p are the stress and the plastic strain. ρ_I, l_I and ξ_I are the density of I constituent, latent heat produced by I constituent, and the volume fraction of the I constituent, in that, the sum of the volume fractions of the I constituent (pearlite and bainite phases, martensite, and retained austenite) is 1 [7–10].

Based on Fourier's law of heat conduction, the equation is as follows:

$$q_I = -\lambda \frac{\partial T}{\partial \chi_I} \vec{n} \tag{4}$$

In Equation (5), λ, T and χ_I are the coefficient of heat conduction, the temperature, and the properties of the I constituents. The $\vec{n}$ is the direction vector of heat transfer. Consider the convective heat transfer boundary between the part and the quenching medium during quenching and list the boundary conditions as follows [7–10]:

$$-\lambda \frac{\partial T}{\partial \chi_I} \vec{n} = h(T - T_{oil}) \tag{5}$$

In the formula, λ , T and χ_I are the coefficient of heat conduction, the temperature, and the properties of the I constituents. The $\vec{n}$ is the direction vector of heat transfer. The h, T and T_{oil} are the heat transfer coefficient, real-time part temperatures, and the temperature of the coolant in quenching, respectively.

However, as a temperature-time curve was measured in the cooling curves in the heat-treatment experiment that reflected the temperature of the probe core and a sensor at a fixed position, it is difficult to make a quantitative assessment of the difference in the cooling state of a different surface from this point of the cooling curve alone, and was used in the simulation; whereas, the heat transfer coefficient is a reflection of the rate of heat transfer from the surface. Compared to the cooling curve, the heat transfer coefficient is a more intuitive reflection of the variation in the quenched capacity of the medium and is one of the process conditions that has the greatest influence on the results of numerical quenching simulations. Due to the time and temperature differences between the surfaces in contact with the quenching oil, it was assumed that there is a time difference between the quenching process and the breakage of the oil film in contact with each surface, i.e., there is a certain time difference in the peak temperature at which the maximum heat transfer coefficient is obtained—a numerical simulation work program was developed for three different forms of heat transfer, axial symmetry heat transfer, orthogonal symmetrical heat transfer, and external orthogonal internal axial symmetry heat transfer. Axial symmetry heat transfer is all surfaces of the bearing outer ring that are applied with the same heat transfer boundary conditions. The orthogonal symmetrical heat transfer that has different heat transfer boundary conditions, is applied to the two sets of orthogonal symmetrical surfaces of the bearing outer ring. External orthogonal symmetrical and internal axial symmetry heat transfer is when different heat transfer boundary conditions are applied to the two sets of orthogonal symmetrical external surfaces of the bearing outer ring, and the same heat transfer boundary condition is applied to all internal surfaces of the bearing outer ring. According to the cooling curve of the quenching oil in Figure 5, two heat transfer coefficients were set (there is a certain time difference between the two heat transfer coefficient rules), as shown in Figure 7 [4,11,21,22].

In Figure 7, the two different colors represent the different heat transfer coefficient taken rules, which should also correspond to the rule when the heat transfer boundaries are set. The red curve is obtained from the cooling curve by the No. 1 thermocouple (ch1 curves) according to the concentrated heat capacity method, and the green curve is obtained from the cooling curve by the No. 2 thermocouple (ch2 curves). Heat transfer boundaries were set, as shown in Figure 8.

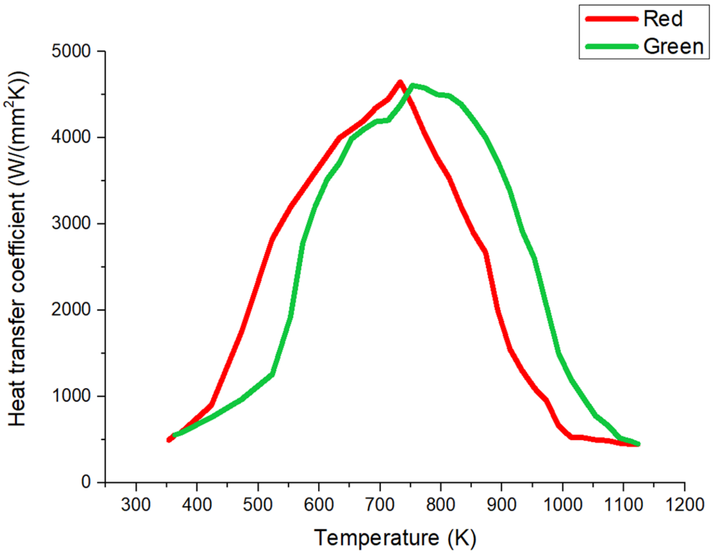

Figure 7. Heat transfer coefficients used in numerical simulation.

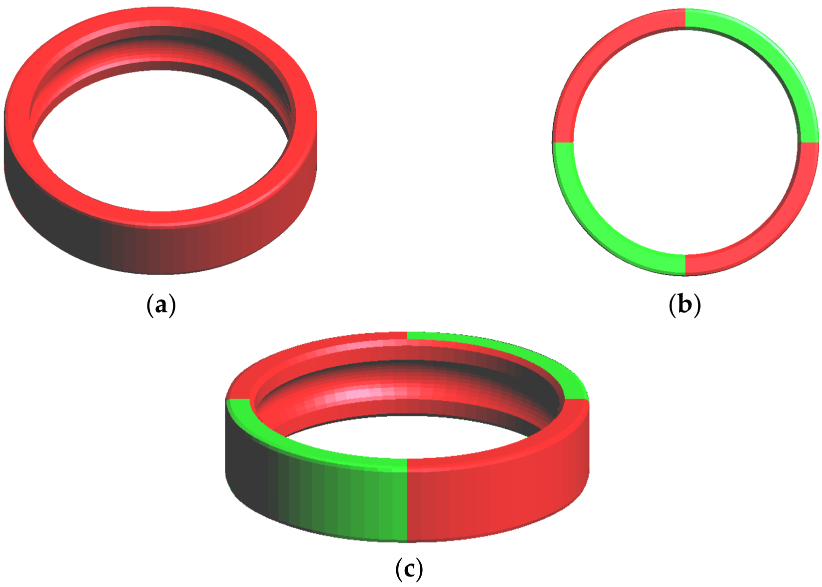

Figure 8. Heat transfer boundaries: (**a**) axial symmetry heat transfer; (**b**) orthogonal symmetrical heat transfer; (**c**) external orthogonal symmetrical and internal axial symmetry heat transfer.

2.5. Material Analysis

The chemical compositions of the GCr15 steel are shown in Table 3.

Table 3. The chemical compositions of the GCr15 steel (wt.%).

Fe	C	Si	Mn	Cr	Cu	Mo	Ni + Cu	P	S
Bal.	0.95~1.05	0.15~0.35	0.25~0.45	1.4~1.65	≤0.25	≤0.1	≤0.5	≤0.025	≤0.025

Bearing steel GCr15 has a commonly used bearing material, but all the thermal physical properties and mechanical properties that have changed with the temperature involved in the heat treatment of GCr15 could hardly be retrieved in the past literature. To this end, we used the material design software JMatPro [23] to calculate the thermal properties and mechanical properties of GCr15, and at the same time, we calculated the continuous cooling curve (CCT) of GCr15. The thermal physical properties and mechanical properties of each phase, such as the thermal conductivity, thermal expansion coefficient, specific heat, Poisson's ratio, Young's modulus, yield stress, and hardening parameter, were obtained by JMatPro and are shown in Figure 9.

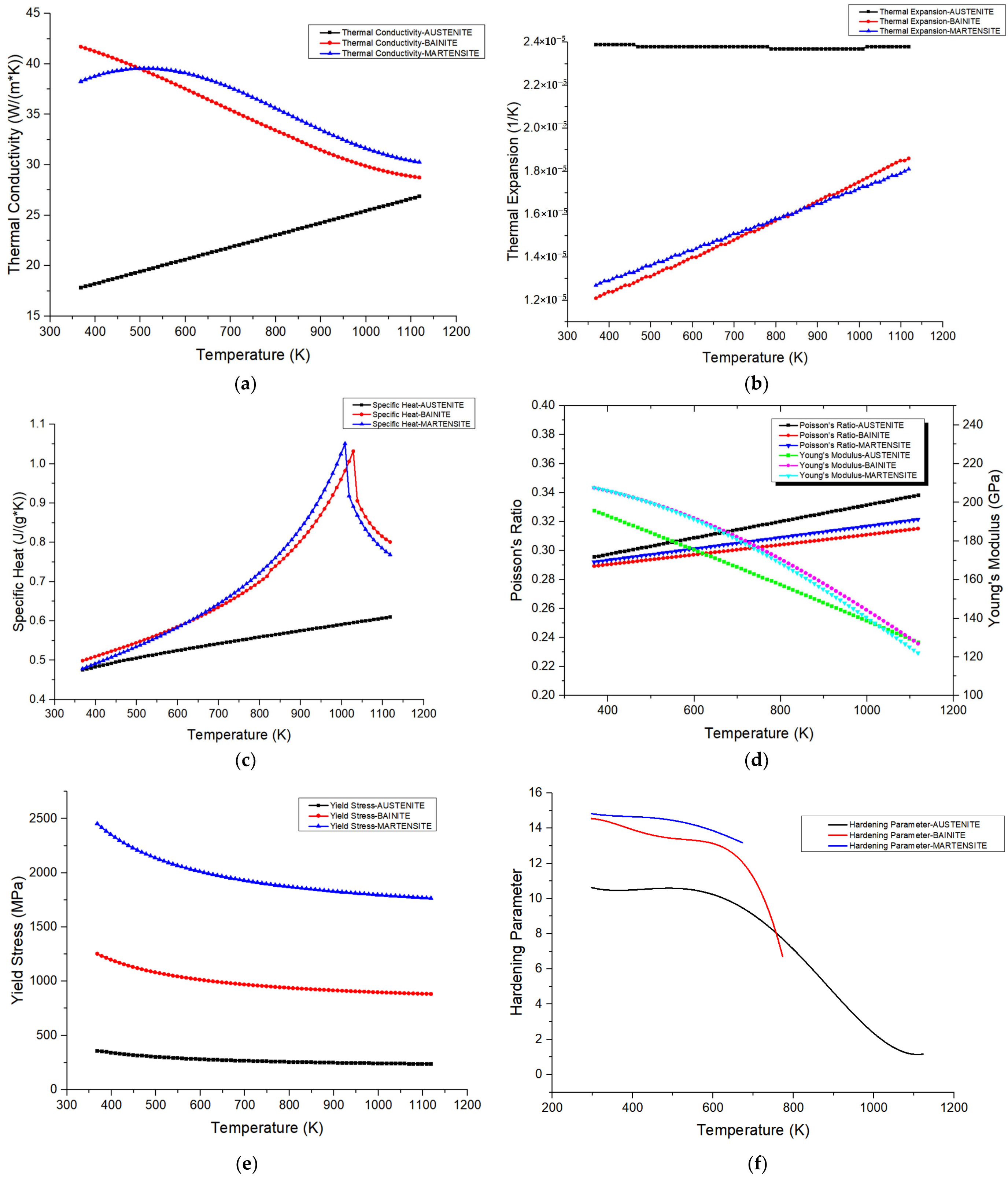

Figure 9. *Cont.*

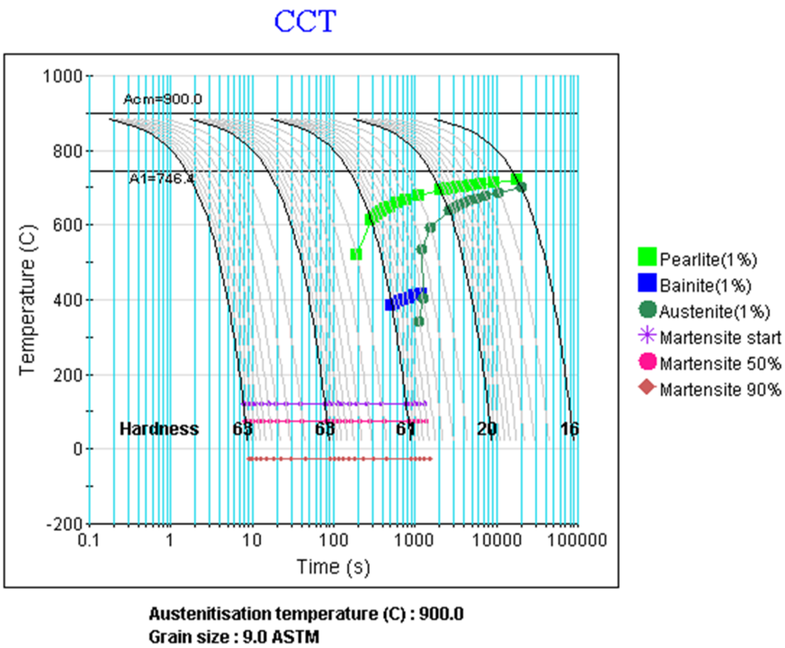

(g)

Figure 9. GCr15 thermal physical properties and mechanical properties: (**a**) thermal conductivity; (**b**) coefficient of thermal expansion; (**c**) specific heat; (**d**) Poisson's ratio and Young's modulus; (**e**) yield stress; (**f**) hardening parameter; (**g**) continuous cooling curve of GCr15.

With the application of a multi-functional thermal load testing machine, it finished the transformation plasticity experiments and collation of data to obtain each phase-change expansion coefficient and phase-change plasticity coefficient, as shown in Table 4 [6].

Table 4. GCr15 coefficient of phase expansion and coefficient of phase plasticity.

Bainite Coefficient of Phase Expansion	Martensite Coefficient of Phase Expansion	Bainite Coefficient of Phase Plasticity	Martensite Coefficient of Phase Plasticity
2.01×10^{-3}	5.03×10^{-3}	9.952×10^{-5}	7.519×10^{-5}

3. Results and Discussion

The simulation results of the set axial symmetry heat transfer boundaries are shown in Figure 8a. It obtained the temperature distribution by axial symmetry heat transfer set during quenched from Figure 10. Figure 10a was used to reflect the change of temperature with the time during quenching. The red curve was attained by taking the boundary point at the inner surface of the outer ring; the black curve was taken at the center of the section; the blue curve was taken at the boundary of the outer surface of the outer ring. It can be concluded, therefore, that all the surfaces were set with the same heat transfer coefficient rule and that the cooling rate of the outer circumferential surface and the inner circumferential surface was almost identical. Due to the center of the section had no direct contact with oil or the temperature transfer, which was mainly heated conduction; therefore, its cooling rate was more lower.

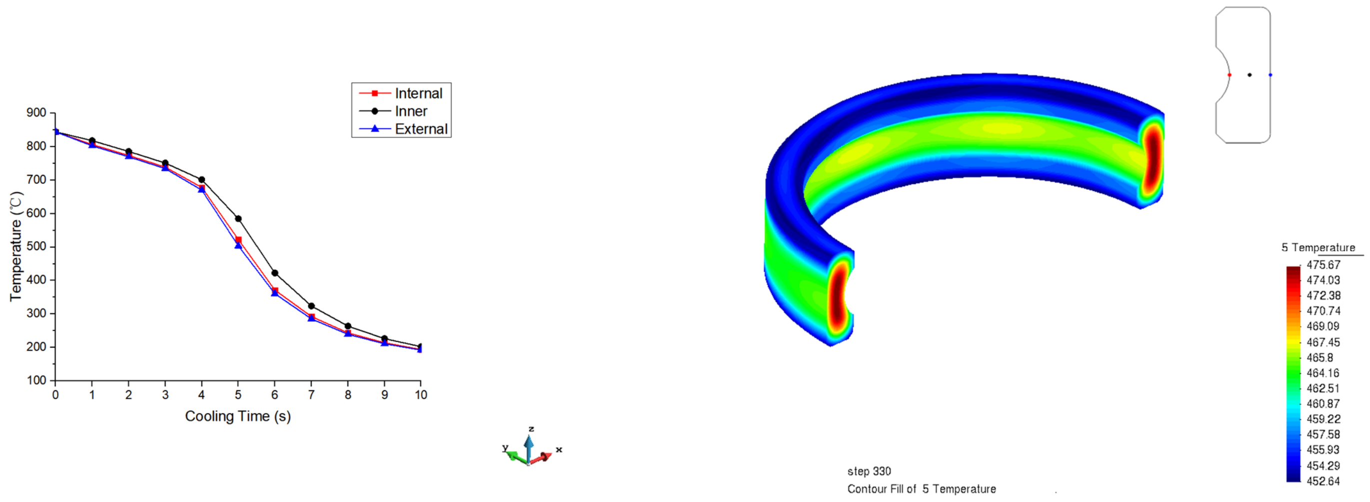

(**a**) (**b**)

Figure 10. Analysis of the temperature field for axial symmetry heat transfer. (**a**) Temperature versus time curve during quenching; (**b**) temperature field at 10 s quenching.

From about 5 s to 6 s, the maximum rate occurred, with peaks occurring in this range. As time passed, the decrease in the heat transfer coefficient and effects from the latent heat of the phase transition caused the cooling rate to gradually decrease and level off. As can be seen from the cloud diagram in Figure 10b, for quenching at 10 s, the temperature difference between the center of the section and the circumferential surface was more obvious due to the small distance of the part cores from the inner and outer surfaces, with a linear spacing of 2 mm. The temperature trend on the inner and outer surfaces was slower than on the top and bottom surfaces of the part.

The effect of this temperature field distribution on deformation is as shown in Figure 11.

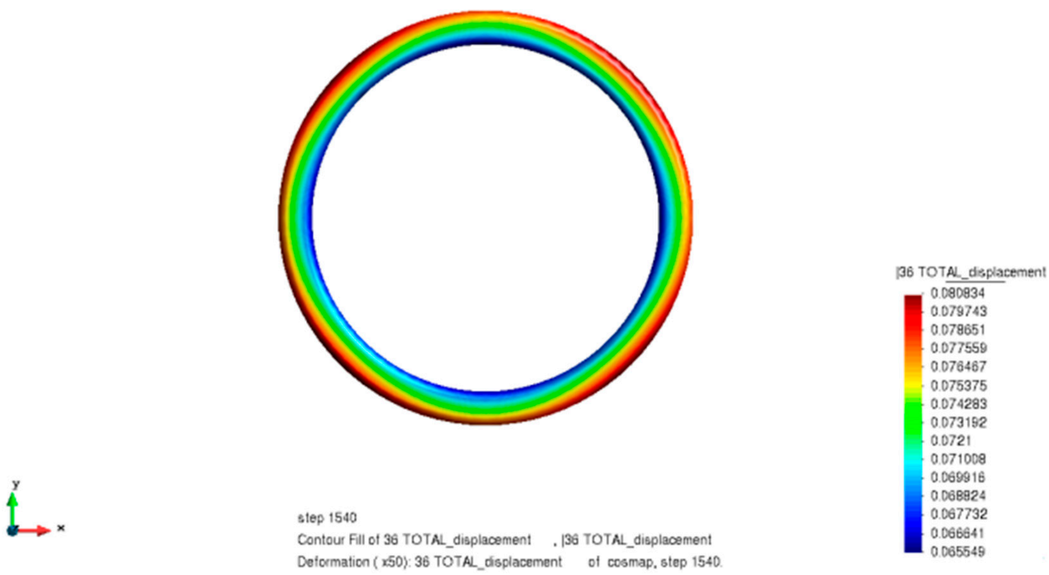

Figure 11. Deformation (×50) by axial symmetry heat transfer.

From Figure 11, it is obtained that each area of the bearing outer ring deformation was relatively uniform, the deformation trend was close to axial symmetry distribution, and the maximum value was approximately 0.08 mm. When the model was enlarged by 50 times, it still presented a round shape. In order to compare the results with the experiment, we referred to the method of height selection in the ellipticity measurement experiment; four quadrants on the outer surface were measured at different height positions, as shown in

Figure 12. The *X*-axis represents the part height position and the *Y*-axis represents the deformation value of each quadrant point in different height positions. At any height position, the deformation values of the four quadrant points were almost equal. This proves again, from the result, that there is uniform deformation in the circumferential direction by axial symmetry heat transfer.

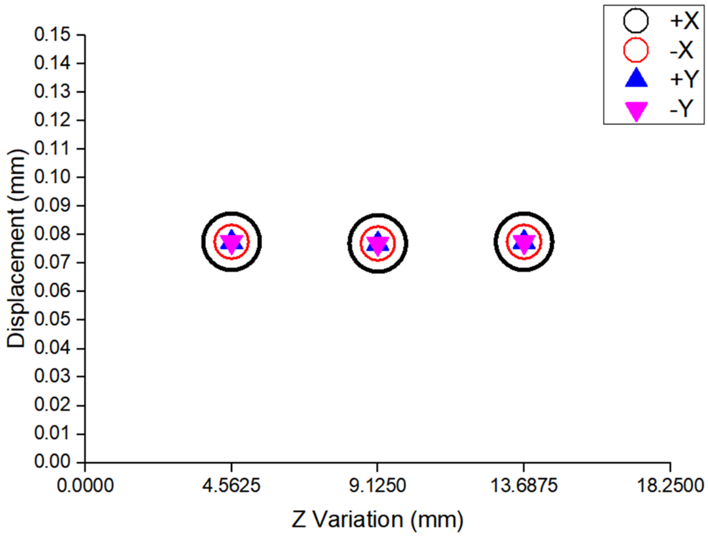

Figure 12. Deformation value of each quadrant point in different height positions for axial symmetry heat transfer.

Based on the above results, the ellipticity values in different height positions were calculated by axial symmetry heat transfer, as shown in Table 5. After quenching, the ellipticity values of the bearing outer ring were almost omitted.

Table 5. Ellipticity in axial symmetry heat transfer simulation (mm).

Quarter Height of Part	Half-Height of Part	Three-Quarter Height of Part
0.0002	0.0002	0.0002

It can be concluded, therefore, that all axial symmetry surfaces of the bearing outer ring were applied with the same heat transfer boundary condition; deformation was more uniform and little elliptical deformation after quenching occurred, thus, this is an ideal state. In order to study the causes of elliptical deformation of the bearing outer ring after quenching, the other two different heat transfer boundary forms were applied, as demonstrated in Figure 8b,c. Figure 8b represents the orthogonal symmetric heat transfer, which was a typical design, and its analysis results symbolize the surface heat transfer asymmetry in the circumferential direction of all the surfaces during oil quenching. The main step for setting the heat transfer boundaries that the bearing outer ring model was placed under, was the Cartesian coordinate system to divide it into quadrants. In one quadrant, the heat transfer law of the inner and outer surfaces was the same. The value rules of adjacent quadrants are different. Figure 8c shows the orthogonal symmetric heat transfer on the outer surface and the axial symmetry heat transfer on the inner surface, which was another typical design. Its analysis results symbolize the surface heat transfer asymmetry in the circumferential direction of only one surface (refer to Figure 8b,c for the boundaries set, the simulated bearing outer ring quenching, and the temperature field and ovalness).

Figure 13a,b reflects the temperature field change with the orthogonal symmetric heat transfer boundaries being set. Figure 13c,d reflects the temperature field change with the external orthogonal symmetrical and internal axial symmetry heat transfer boundaries being set.

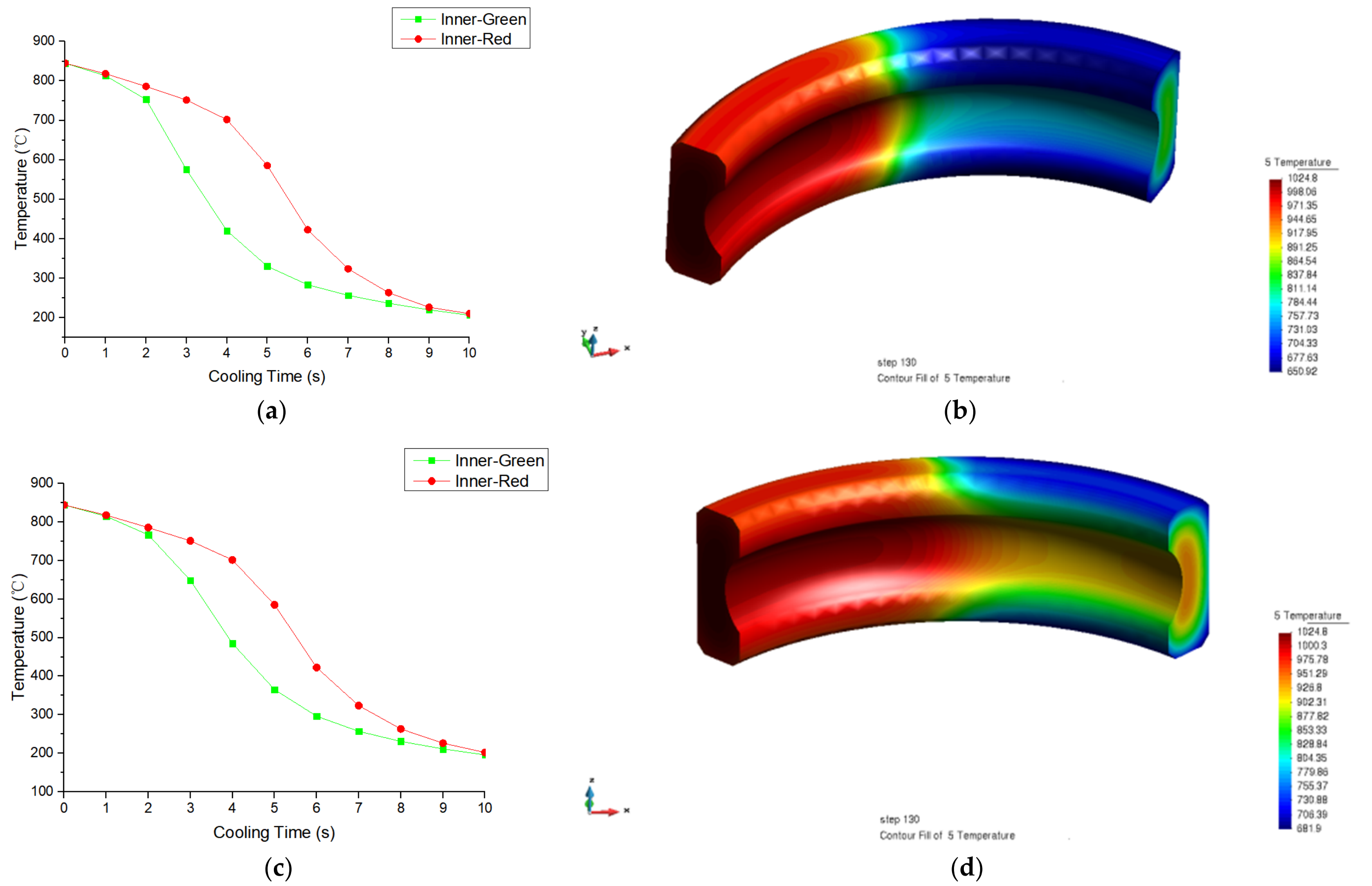

Figure 13. Analysis of the temperature field for orthogonal symmetrical heat transfer and external orthogonal symmetrical, internal axial symmetry heat transfer. (**a**) Cooling curve from center of the two sections for orthogonal symmetrical heat transfer; (**b**) temperature field plot for orthogonal symmetrical heat transfer at 3 s; (**c**) cooling curve from center of the two sections for external orthogonal symmetrical and internal axial symmetry heat transfer; (**d**) temperature field plot for external orthogonal symmetrical and internal axial symmetry heat transfer at 3 s.

In the coordinate system, by intercepting the bearing outer ring model with a 45-degree line and 135-degree line, the center point of the two geometric sections was taken, the temperature field change at the two points during the quenching process was analyzed, and the temperature cooling curve with time was constructed, as shown in Figure 13a,c. The upper model in the 45-degree line and 135-degree line area was intercepted, and its temperature distribution is presented in the form of a cloud picture, as shown in Figure 13b,d.

From Figure 13a, the green curve has shown the effect on temperature by applying the green heat transfer coefficient rule shown in Figure 7, while the red curve has indicated the application of the red heat transfer coefficient rule in Figure 7. As the green curve heat transfer coefficient reaches its peak first and the red slightly later, there is a certain time difference. Therefore, the cooling rate of the green curve was faster than the red one. The maximum rate of the green curve occurred in about 2 to 3 s, with peaks occurring in this range. However, the red curve reached the above details between 5 s and 6 s. Under the different heat transfer conditions, the temperature changed over time, which was already different. Comparing Figures 10a and 13a, the rule of the black curve in Figure 10a and the rule of the red curve in Figure 13a were in agreement, which leads to the conclusion that under the same heat transfer conditions, the temperature changed with time is already almost the same. In summary, the change in the heat transfer coefficient has affected the change in the temperature field.

The cloud plot in Figure 13b shows that the heat transfer process in quenching took place firstly in the right half and later in the left half. This result can match the heat transfer law of the two curves in Figure 7. The temperature gradient in the annular direction was obviously produced, and the temperature distribution boundary and the heat transfer boundary were close to coinciding. This verified that the time difference between the bearing outer ring's two surfaces of oil-film rupture during the quenching process could create a temperature gradient. Combined with Figure 10b, heat transfer asymmetry in the circumferential direction on each circumferential surface has caused an uneven temperature distribution in the circumferential direction.

From Figure 13c, the green curve shows the comprehensive effect on temperature when different heat transfer rules are set on the inner and outer surfaces. The red one has indicated the temperature change under the influence of the red heat transfer coefficient rule in Figure 7. However, the cooling rate of the green curve was faster than the red one, about 2 to 3 s, where the maximum rate of the green curve occurred, with peaks occurring in this range. The red curve reached the above details between 5 and 6 s, however, the zone area which was formed between the green curve and red curve was smaller in Figure 13c than in Figure 13a. The area of the intersecting area of two curves can be mathematically expressed as the integral of the temperature difference at the analysis point in the time range.

The cloud plot in Figure 13d shows that the heat transfer process in quenching took place firstly in the right half and later in the left half; the temperature gradient in the annular direction was obviously produced. Compared with Figure 13b, the right half of the model was affected by the heat transfer coefficient of the inner surface, and the heat transfer speed on the inner surface was slower. Combined with the analysis in Figure 13b,d, as long as there was a circumferential surface with different heat transfer laws, that is, the oil film ruptured was uneven in a certain circumferential direction, it produced a temperature gradient in the annular direction.

Summarizing all the analyses presented in Figure 13, the presence of the crossover region could indicate the presence of a temperature gradient in the annular direction. When different heat transfer conditions were set on any circumferential surface, it created a temperature gradient in the annular direction. The size of the area may be related to the value of the ellipticity of the outer ring of the bearing after quenching. This needs to be verified in the deformation simulation.

The effect of temperature field distribution on deformation is shown in Figure 14. The bearing outer ring has occurring non-axisymmetric deformation.

Figure 14 shows a magnified 50× deformation plot after quenching. After quenching, it has deformed to a greater extent in the negative 45-degree direction, and to a lesser extent, in the 45-degree direction, an elliptical form is shown.

Because the annular temperature gradient appeared in quenching, this made it load larger compressive stresses in the negative 45-degree direction and load smaller compressive stresses in the 45-degree direction, just as Figure 15 shows.

The ellipticity is calculated in 45-degree and negative 45-degree directions. The maximum and minimum deformation in different height directions is shown in Figure 16 and the ellipticity is calculated, as shown in Table 6.

Table 6. Ellipticity results in simulation (mm).

Z Variation	Orthogonal	External Orthogonal Internal Symmetric
3/4H	0.14	0.158
1/2H	0.14	0.158
1/4H	0.14	0.158

Figure 16 shows that the bearing outer ring deformation has a maximum and minimum value in the circumferential direction by different heat transfer boundary conditions, which are applied to different surfaces of the bearing outer ring. It forms the ellipticity in the circumferential direction.

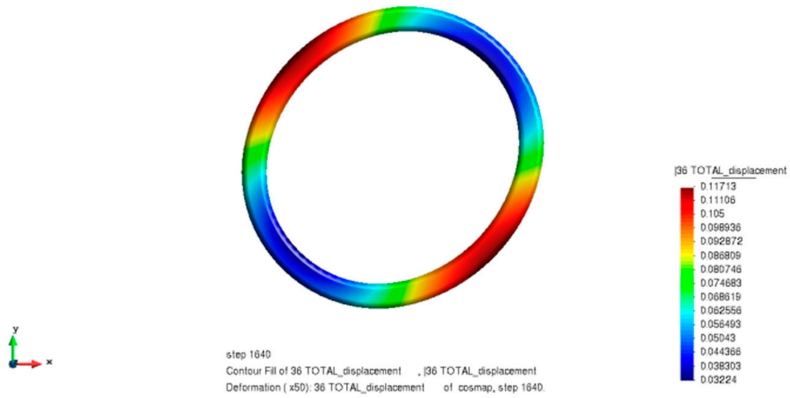

(**a**)

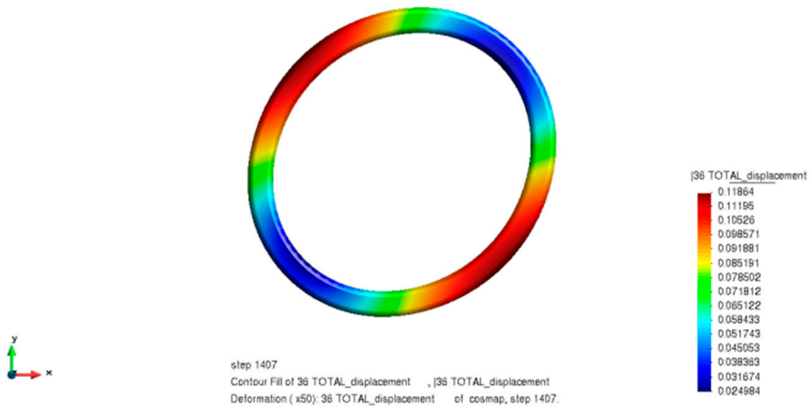

(**b**)

Figure 14. Deformation (×50) by orthogonal symmetric heat transfer and orthogonal symmetric heat transfer on the outer surface, axial symmetry heat transfer on the inner surface. (**a**) Deformation (×50) by orthogonal symmetry heat transfer; (**b**) deformation(×50) by orthogonal symmetric heat transfer on the outer surface and axial symmetry heat transfer on the inner surface.

Table 6 shows that with applied orthogonal symmetrical heat transfer, the ellipticity was 0.14 mm, and with applied external orthogonal symmetrical and internal axial symmetry heat transfer, the ellipticity was 0.158 mm. Because the former for the newly added boundary conditions resulted in a residual stress value of about 42 MPa, while the latter, due to the internal surface still maintained axial symmetry, the newly added boundary conditions are only applied to the external surface of the bearing outer ring; therefore, the residual stress value is about 30 MPa. The residual stress value on the circumferential surface is different, causing an ellipse of the bearing outer ring. The analysis of the temperature cooling curves mentions the size of the area where the curves cross as a possible reason for the value of ellipticity, and thus, here it was also confirmed.

Combining Table 5 with Table 6, it can be concluded that when all surfaces applied the same heat transfer law, an annular temperature gradient was formed, and the ellipticity results of the simulation are little and almost invisible. However, the surfaces applied with two or more heat transfer boundary conditions created a temperature gradient in the annular direction, and resulted in orthogonal residual thermal stress, leading to form non-axisymmetric deformation, and the bearing outer ring presented an elliptical shape. The ellipticity results of the simulation are closer to the experimental situation in Table 1. The conclusion shows that the two types of assumed non-axisymmetric cases develop a judgment on the formation mechanism of the elliptic bearing outer ring after quenching. The actual simulation needs to obtain the rule of heat transfer coefficients on each surface of the part before the simulation can produce data consistent with the experimental results.

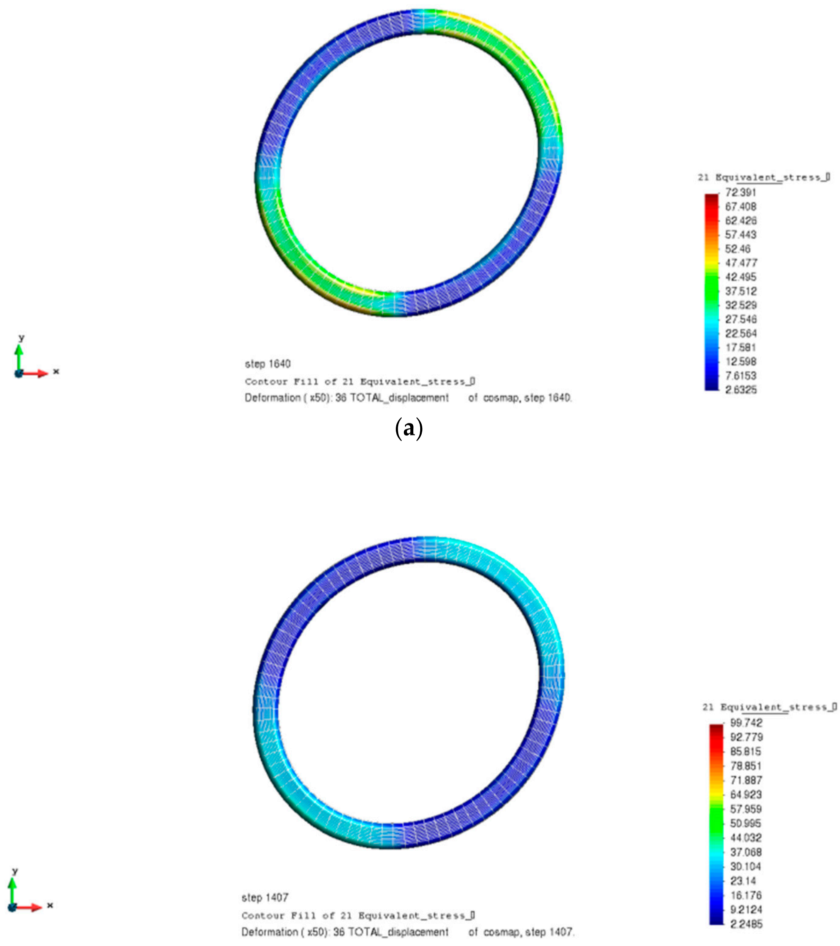

(**a**)

(**b**)

Figure 15. Residual stress for orthogonal symmetrical heat transfer, external orthogonal symmetrical and internal axial symmetry heat transfer (50× deformation as a reference). (**a**) Residual stress for orthogonal symmetrical heat transfer; (**b**) residual stress for external orthogonal symmetrical and internal axial symmetry heat transfer.

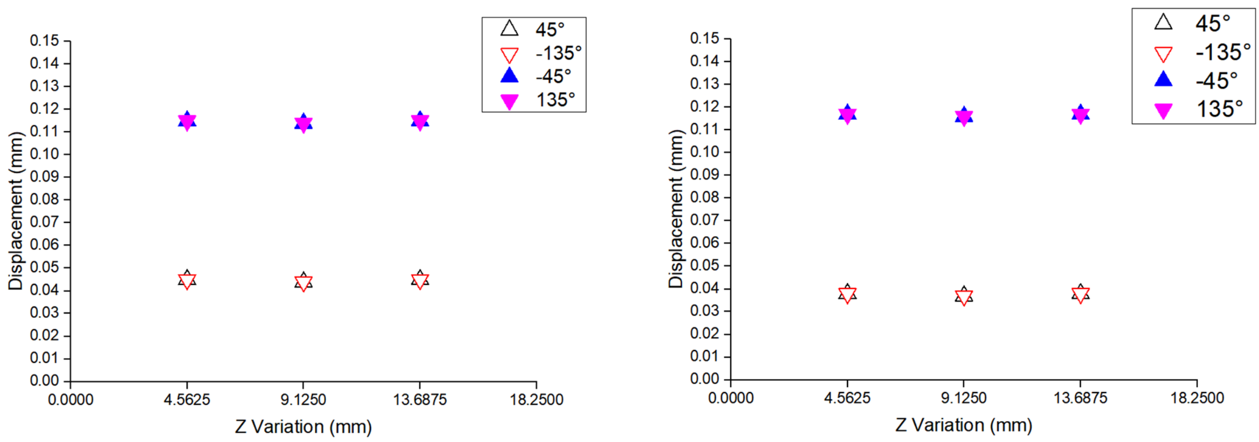

(**a**) (**b**)

Figure 16. Maximum and minimum deformation in different height directions. (**a**) Results of orthogonal symmetrical heat transfer; (**b**) Results of external orthogonal symmetrical and internal axial symmetry heat transfer.

4. Conclusions

1. With applied orthogonal symmetrical heat transfer, the ellipticity was 0.14 mm, and with applied external orthogonal symmetrical and internal axial symmetry heat transfer, the ellipticity was 0.158 mm. The experimental value was 0.83–0.96 mm, and both are closer to the experimental situation. This indicates that the simulation solution is appropriate and that the assumption of the heat transfer boundaries is reasonable.
2. By using one or more heat transfer boundary conditions on the surfaces of the bearing outer rings, we achieved a simulation of the bearing outer ring, and, thus, experimental results were compared. From the analysis of the temperature and deformation results by setting the same heat transfer boundary condition, temperature cooling from the outside to inside was reflected; with the center cooling the slowest, where the resulting deformation appeared more uniform and, therefore, this part showed little elliptical form after quenching.
3. When different heat transfer boundary conditions are applied to the two sets of orthogonal symmetrical surfaces of the bearing outer ring, heat from the bearing outer ring makes the oil film on its surfaces reach a boiling state in succession until the film of the surface breaks in order. The rupture of the steam film has a time difference; it causes the formation of temperature gradients and creates orthogonal residual stress in the annular direction, which ultimately makes the bearing outer ring occur with non-axisymmetric deformation, generating shape tolerances for ellipticity. By comparing the experimental results, the results of the simulation analysis were verified.
4. According to the research in this paper, it can be demonstrated that improving the uniformity of the heat transfer coefficient in the circumferential direction is key to avoiding elliptical deformation of the bearing. For this reason, our suggestion is to increase the stirring cooling method in the oil tank, so that the heat transfer coefficient in the circumferential direction of the bearing is more uniform, therefore making it possible to reduce elliptical deformation.

Author Contributions: Conceptualization, D.J. and Q.L.; methodology, D.J. and Q.L.; software, D.J.; validation, Q.L. and D.J.; formal analysis, Q.L.; investigation, W.L. and M.Z.; resources, W.L. and M.Z.; preparation of specimens for the experiment, X.L., K.I. and Q.L.; data curation, Q.L. and X.L.; data acquisition, R.L. and K.I.; development of heat transfer coefficient calculation program, R.L. and D.J.; analytical method of heat transfer coefficient, D.J.; writing—original draft preparation, Q.L.; writing—review and editing, D.J. and Q.L.; project administration, D.J. All authors have read and agreed to the published version of the manuscript.

Funding: This research was funded by the National Key Research and Development Project (2018YFE0207000).

Institutional Review Board Statement: Not applicable.

Informed Consent Statement: Not applicable.

Data Availability Statement: Data is contained within the article.

Acknowledgments: The authors thank Changzhou NRB Corporation in China and the High-Tech Research Center in Saitama Institute of Technology in Japan for the related experiments.

Conflicts of Interest: The authors declare no conflict of interest.

References

1. Chidester, A.J.; Darrang, C.V.; Hoff, R.C.; Imundo, J.R.; Maloney, J.L. *Heat Treatment of Bearings*; ASM International: Almere, The Netherlands, 2014; Volume 4.
2. Zhang, X.; Li, Z.; Cui, X. Numerical simulation on heat treatment deformation of GCr15 bearing rings. *Bearing* **2020**, *11*, 45–49.
3. Xue, M. Effect of austenitization condition on microstructure of hypereutectoid steel. *Foundry Technol.* **2014**, *12*, 2857–2859.
4. Narazaki, M.; Shichino, H.; Sugimoto, T.; Watanabe, Y. Validation of Estimate Heat Transfer Coefficients during Quenching of Steel Gear. In Proceedings of the Fifth International Conference on Quenching and the Control of Distortion, Berlin, Germany, 23–25 November 2007; pp. 111–117.

5. Inoue, T.; Ju, D.Y.; Arimoto, K. Metallo-Thermo-Mechanical Simulation of Quenching Process-Theory and Implementation of Computer Code "Hearts". In Proceedings of the First International Conference on Quenching and Distortion Control, Chicago, IL, USA, 22–25 September 1992; pp. 205–212.
6. Ju, D.-Y.; Inoue, T. On the material process simulation code COSMAP simulated examples and its experimental verification for heat treatment process. *Mech. Behav. Mater. X* **2007**, *345–346*, 955–958.
7. Deng, X.; Ju, D.Y. Modeling and Simulation of Quenching and Tempering Process in steels. In Proceedings of the International Federation for Heat Treatment and Surface Engineering 20th Congress, Beijing, China, 23–25 October 2012; pp. 23–25.
8. Ju, D.Y.; Zhang, W.M. Modeling and experimental verification of plastic behavior of the martensitic transformation plastic behavior in a carbon steel heat treatment of materials. *Solid State Phenom.* **2006**, *118*, 369–374. [CrossRef]
9. Watanabe, Y.; Ju, D.Y. Cooperative research to optimize heat treating process condition by computer based technology. *Heat Treat. Mater.* **2006**, *118*, 349–354.
10. Maio, S.; Wang, J. Improvement and analysis of fatigue strength for mild steel 20MnCrS5 during carburizing and quenching. *Mater. Sci. (Medžiagotyra)* **2020**, *26*, 192–198. [CrossRef]
11. Miao, S.; Ju, D.Y.; Chen, Y.; Liu, L. Optimization based on orthogonal experiment design and numerical simulation for carburizing quenching process of helical gear. *Mater. Perform. Charact.* **2019**, *8*, 66–79. [CrossRef]
12. Xusheng, L.; Dongying, J.; Jianting, C.; Sirui, W.; Yong, C.; Fangbo, H.; Hui, L. Effect of transformation plasticity on gear distortion and residual stresses in carburizing quenching simulation. *Coatings* **2021**, *11*, 1224. [CrossRef]
13. Wang, J.; Yang, S.; Li, J.; Ju, D.; Li, X.; He, F.; Li, H.; Chen, Y. Mathematical Simulation and experimental verification of carburizing quenching process based on multi-field coupling. *Coatings* **2021**, *11*, 1132. [CrossRef]
14. Li, M.; Deng, K.; Deng, S.; Kang, N. FEM analysis of a new type hub bearing rings during quenching. *Bearing* **2017**, *1*, 24–28.
15. Yiyu, S.; Wenfei, P.; Shaoqiang, C. Effect of cold treatment process on roundness of bearing ring. *Mater. Res. Express* **2022**, *9*, 026513.
16. Zhaoxi, C.; Zhiyue, S.; Feng, Y.K.S.; Wenquan, C.; Yuqing, W. Effects of double quenching on fatigue properties of high carbon bearing steel with extra-high purity. *Int. J. Fatigue* **2019**, *128*, 11.
17. Xiaohui, L.; Dongsheng, Q.; Wei, L.; Xuejun, J. Enhanced toughness of bearing steel by combining prior cold deformation with martensite pre-quenching and bainite transformation. *Mat. Lett.* **2019**, *234*, 5–8.
18. Kai, Z.; Baiqing, X.; Xiwu, L.; Yongan, Z.; Li, Z.; Li, Y.; Wen, K.; Yan, L. Finite element simulation on residual stress during immersion quenching and pre-stretching of Al7055 thick plates. *Mater. Res. Express* **2022**, *9*, 026525.
19. Wu, H.Y.; Han, D.X.; Du, Y.; Gao, X.H.; Du, L.X. Effect of initial spheroidizing microstructure after quenching and tempering on wear and contact fatigue properties of GCr15 bearing steel. *Mater. Today Commun.* **2022**, *30*, 3. [CrossRef]
20. Chang, G.; Liu, X.; Chen, C.; Ren, R. Calculation of the heat transfer coefficient of GCr15 steel in quenching process. *Mater. Guide* **2013**, *21*, 120–122.
21. Ju, D.Y.; Ichtani, K.; Nakamura, E.; Mukai, R. Heat treatment and surface engineering. *AIM* **1998**, *2*, 283–291.
22. Kanamori, H.; Ju, D.Y. Identification of heat transfer coefficients and simulation of quenching distortions on disk probe. *Mater. Trans.* **2020**, *61*, 884–892. [CrossRef]
23. Saunders, N.; Guo, U.K.Z.; Li, X.; Miodownik, A.P.; Schillé, J.-P. Using JMatPro to model materials properties and behavior, Industrial Insight. *JOM* **2003**, *55*, 60–65. [CrossRef]